Electrical Power and Energy Systems 114 (2020) 105395

Contents lists available at ScienceDirect

Electrical Power and Energy Systems

journal homepage: www.elsevier.com/locate/ijepes

Adaptive direct power control for double fed induction generator used in wind turbine

Farida Mazouz[a,*], Sebti Belkacem[a], Ilhami Colak[b], Said Drid[c], Youcef Harbouche[a]

[a] LEB, Department of Electrical Engineering, University of Batna 2, Algeria
[b] Electrical and Electronics Engineering Department, Nisantasi University, Turkey
[c] LSPIE Laboratory, Electrical Engineering Department, University of Batna 2, Algeria

ARTICLE INFO

Keywords:
Wind energy conversion system (WECS)
Doubly fed induction generator (DFIG)
Direct power control (DPC)
Adaptive direct power control (A-DPC)
Vector control (VC)
Parameter variations

ABSTRACT

This papers deal with a new Adaptive Direct Power Control for Doubly-Fed Induction Generator of 1.5 MW. The main feature of the proposed strategy is based on the replacement of the fixed switching table by an adaptive one. The online update of the adaptive switching table depends on the reactive power variation and past switching sequences. The proposed adaptive direct power control is compared with Vector Control and Classical Direct Power Control. The robustness of the proposed control scheme against parameter, load and wind speed variations have done with success. The main performance of the Adaptive Direct Power Control strategy is the reduction of powers ripples, thus reduce of torque ripple on the shaft of the turbine.

1. Introduction

Doubly fed induction generators (DFIG) are used widely in wind generation systems because of their variable speed operation [1–7]. There are several works addressed to the statistical analysis regarding the integration of DFIG based wind power systems into the power grid on the topics of stability, power quality and energy-efficiency [8–9].

The instantaneous control of the active and reactive powers of the stator of DFIG is obtained by regulating the decoupled rotor currents, using a proportional integral controller (PI) [10–14]. However, this control structure depends on the parameters of the Induction Generator and therefore it requires several control loops and need many computational efforts to guarantee the stability of the structure over the entire speed. Many methods have been presented to remedy the aforementioned difficulties. The Direct Torque Control (DTC) or Direct Power Control (DPC) has been introduced [15–22]. In the DTC, the flux and the torque are controlled directly, while in DPC, active and reactive powers are controlled directly by selecting an appropriate command. The DPC has been suggested to the DFIG and has many advantages over the conventional VC scheme, such as not requiring synchronous coordinated transformations, no current loops, less parameters dependence and relatively easy implementation. The classical DPC are subject to considerable ripples in currents, active and reactive powers and the switching frequency is not constant.

Various controls have focused on the development of DPC methods that work at a constant switching frequency using space vector modulation (DPC-SVM) [23–26]. Its main feature is the removal of hysteresis regulators and switching table, eliminating the problems associated with it. Reduction of power pulsation and power quality was achieved. These controllers are not robust against parameters uncertainty.

Authors in Refs. [27] and [28] are interested in DPC without zero voltage sequences; a first choice is to use only active sequences. This choice has the advantage of simplicity and avoids the randomness related to the direction of variation of the powers when applying a zero sequence. Indeed, the use of these voltages sequences the switching frequency can be reduced.

Various methods are studies using non-linear control laws such as feedback linearization [29–30], backstepping [31], intelligent control like fuzzy logic controller [32], neural networks [33]. Several of these control techniques produce very complicated control laws and have rather high computations. These calculations usually depend on system states and several model parameters that have the effect of decrease the control robustness.

Sliding Mode Control (SMC) is designed to uncertain and disturbed nonlinear systems due to its robustness to uncertainties and external disturbances. Much work has been done on (SMC) [34–38]. In [34], the sliding mode controllers are applied to the current controller on the rotor side converter, where the powers control strategy, based on the indirect vector control without powers loops. The combination of (SMC-DPC) reduces power ripple. The authors used the sign function, but this

* Corresponding author.
E-mail address: f.mazouz@univ-batna2.dz (F. Mazouz).

https://doi.org/10.1016/j.ijepes.2019.105395
Received 22 August 2018; Received in revised form 27 May 2019; Accepted 30 June 2019
Available online 10 July 2019
0142-0615/

Nomenclature

Turbine model

v, $\Omega_{turbine}$,Ω_{mec}	wind, turbine and DFIG mechanical speed
P_{aer}	aerodynamic mechanical power
C_p	turbine power coefficient
λ	tip speed ratio
β	pitch angle
R	turbine radius
G	gearbox ratio
J, $J_{turbine}$, J_g	total, turbine and generator inertia
f:	friction coefficient
ρ	air density
T_{aer}, T_{em}, T_g	aerodynamic, electromagnetic, generator torque
S	wind wheel area
$V_{\alpha s}$, $V_{\beta s}$,	stator voltages in the α-β axis

DFIG model

V_s, V_r	stator, rotor voltage
I_s, I_r	stator, rotor current
V_{dc}	DC link voltage
φ_s, φ_r	stator, rotor flux
R_s, R_r	stator, rotor resistance
L_s, L_r	stator, rotor inductance
M	mutual inductance
p	number of pole pairs
Ω	rotor speed
P_s, Q_s	stator active and reactive power
$P_{s\text{-}ref}$, $Q_{s\text{-}ref}$	references values of the powers
$P_{s\text{-}error}$, $Q_{s\text{-}error}$	active and reactive powers error
(V_0-V_7)	voltage vectors
ρ_r	flux phase

Superscripts

s	stator reference frame
r	rotor reference frame
*, -ref	reference value

Subscripts

α-β	stationary α-β axis
s,r	stator, rotor
d,q	synchronous d,q axis
A,b,c	three-phase reference
A-DPC	adaptive direct power control
DFIG	doubly-fed induction generator
C-DPC	classical direct power control
VC	vector control
WECS	wind energy conversion system
RSC, GSC	rotor and grid side converter
DTC	direct torque control
AC	alternative current
SVM	space vector modulation
VSC	variable structure control
SMC	sliding mode control
DC	direct current
MPC	model predictive control
THD	total harmonics distortion
PI	proportional integral

function produces a vibration phenomenon and increases the total harmonic distortion of the rotor currents. In practice, the use of the SMC has been limited by the complicated online calculations and chattering problem related to the commutations of the control which can be disturbing for the actuators. Since then, many solutions have been proposed to reduce these oscillations: increase of the switching frequency combines an MPPT using a second-order sliding mode continuous control [39–41].

Different model predictive direct power control (MP-DPC) strategies have been studied and compared [42–43]. The main idea of the MPC is based on the use of a system model to be controlled to predict its output over at a certain horizon, the development of an optimal sequence of future orders satisfying the constraints and minimizing a cost function. The advantage of the MPC is the easy inclusion of non-linearity in the model. The proposed controllers accomplish load reduction and improved power capture optimization. It accordingly allows a good achievement of the design objectives. The main drawback of the MPC is the execution time. It is desirable to be able to predict the dynamic behavior and for this, it is necessary to have a precise knowledge of the constituents of the process. However, the problem is that there is often no precise model of the process. There may be several reasons for this: prior information is incomplete, features vary over time, or unknown disturbances affect the process to be controlled.

Various strategies are applied to regulate the DFIG under an unstable condition [44–47]. The authors used DPC in a DFIG-based wind turbine system under unbalanced grid voltage conditions. A first order low pass filter disturbance observer with a proportional current controller was proposed by [44] which elaborate positive sequence power requirements and independently control negative sequence current components under unbalanced voltage conditions. Double frequency pulsations in the stator reactive power and torque are entirely eliminated during steady-state and transient torque/power step modification when the network voltage is unstable.

This paper focuses on a new adaptive DPC for DFIG with tracking table for reactive power variation. The principle of the proposed scheme is based on the replacement of the fixed switching table by an adaptive one.

2. System description

Fig. 1 depicts the DFIG control based on the WECS. The system consists of three elements: the control part, an electrical part, and a mechanical part. Though, the mechanical element illustrated by a wind turbine, the electrical element includes 1.5 MW DFIG connected to the grid via two back-to-back power converters as the grid-side converter (GSC) and the rotor-side converter (RSC). The RSC is responsible for regulating the rotor currents generated torque such that the required power is developed by the DFIG while the GSC controls the DC-link capacitor voltage. The DC-link capacitor is used as an energy storage element, which transmits the required energy between the generator and the grid. Furthermore, the GSC has the capability to produce or absorb reactive power for voltage support demand. Both converters are usually voltage source converters with IGBT switching elements. The converter produces a three-phase voltage at variable frequency, magnitude and phase voltage.

2.1. Wind turbine modeling

The stored wind kinetic energy is defined by:

$$P_v = \frac{1}{2}.\rho.S.v^3 \quad (1)$$

where:

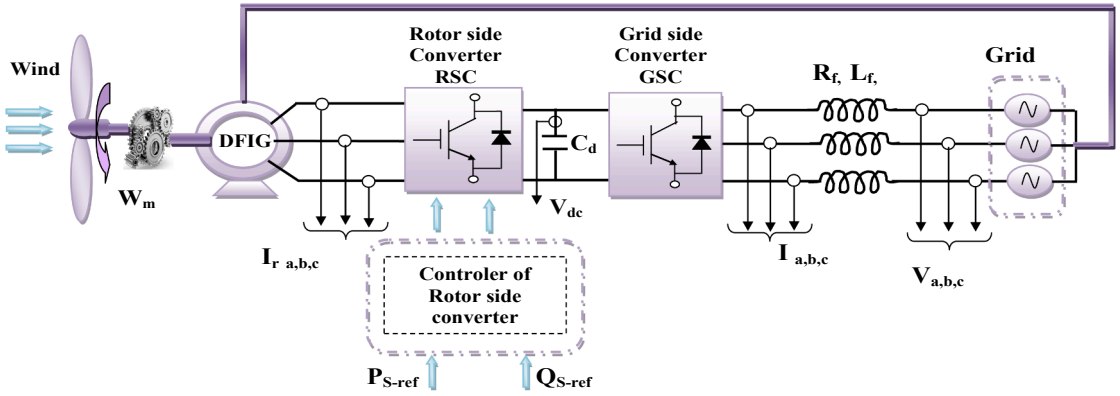

Fig. 1. Block diagram of the wind turbine based DFIG.

S: The wind wheel area (m^2);
ρ: Air density (ρ = 1.225 kg/m^3
v: wind speed (m/s);

The expression of mechanical power from the wind as follows [16]:

$$P_{aer} = C_p.\ P_v = \frac{1}{2}.\ C_p(\beta, \lambda).\ \rho.\ S.\ v^3 \tag{2}$$

where:$C_p$is the turbine power coefficient, λ is the ratio tip speed and β is the pitch angle.

The tip speed ratio is described by:

$$\lambda = \frac{R.\ \Omega_{turbine}}{v} \tag{3}$$

where:

R: Turbine radius;
$\Omega_{turbine}$: Turbine speed;

The aerodynamic torque is expressed by:

$$T_{aer} = \frac{P_{aer}}{\Omega_{turbine}} = C_p(\beta, \lambda).\ \frac{1}{2}.\ \rho.\ S.\ v^3 \frac{1}{\Omega_{turbine}} \tag{4}$$

The total inertia J is composed by the turbine and generator inertia:

$$J = \frac{J_{turbine}}{G^2} + J_g \tag{5}$$

with:

G: Gearbox ratio;
$J_{turbine}$: Turbine inertia;
J_g: Generator inertia.

To characterize the evolution of the mechanical speed, the dynamic equation is applied and can be written as follows:

$$T_g - T_{mec} = J.\ \frac{d\Omega_{mec}}{dt} + f.\ \Omega_{mec} \tag{6}$$

where:

Ω_{mec}: DFIG mechanical speed;
T_{em}: electromagnetic torque;
f: friction coefficient;
T_g: generator torque;

2.2. DFIG model

The DFIG dynamic equations in the reference α-β form are made by [8]. The voltages expressions are given by:

$$\begin{cases} V_{\alpha s} = R_s I_{\alpha s} + \frac{d\varphi_{\alpha s}}{dt} \\ V_{\beta s} = R_s I_{\beta s} + \frac{d\varphi_{\beta s}}{dt} \\ V_{\alpha r} = R_r I_{\alpha r} + \frac{d\varphi_{\alpha r}}{dt} + p.\ \Omega.\ \varphi_{\beta r} \\ V_{\beta r} = R_r I_{\beta r} + \frac{d\varphi_{\beta r}}{dt} - p.\ \Omega.\ \varphi_{\alpha r} \end{cases} \tag{7}$$

The flux equations are given by:

$$\begin{cases} \varphi_{\alpha s} = L_s I_{\alpha s} + M I_{\alpha r} \\ \varphi_{\beta s} = L_s I_{\beta s} + M I_{\beta r} \\ \varphi_{\alpha r} = L_r I_{\alpha r} + M I_{\alpha s} \\ \varphi_{\beta r} = L_r I_{\beta r} + M I_{\beta s} \end{cases} \tag{8}$$

The torque equation is also represented as follows:

$$T_{em} = p.\ (I_{\beta r}.\ \varphi_{\alpha s} - I_{\alpha r}.\ \varphi_{\beta s}) \tag{9}$$

So the supplied active and reactive powers are defined as follows:

$$\begin{aligned} P_s &= (V_{\alpha s} I_{\alpha s} + V_{\beta s} I_{\beta s}) \\ Q_s &= (V_{\beta s} I_{\alpha s} - V_{\alpha s} I_{\beta s}) \end{aligned} \tag{10}$$

3. Control strategies

3.1. Vector control strategy of DFIG

The objective of the vector control of DFIG is to achieve an equivalent system as in DC machines [14], therefore a decoupled control of the active and reactive powers. Indirect vector control is the most used because of its simplicity.

The indirect vector control consists of annulling the quadrature component of the stator flux $\varphi_{qs} = 0$, $and \varphi_{ds} = \varphi_s$.

In this method, decoupling is performed at the output of the rotor current regulators with a feedback from the system. Which allows the adjustment of the powers, one thus distinguishes, a control by loop in cascade of the power and the rotor current for each axis, since it makes it possible to control separately the currents I_{rd}, I_{rq} and the powers Q_s, P_s in closed loop.

The indirect vector control principle is used to generate the corresponding reference voltages V_{rd} and V_{rq}. A Park transformation calculates the rotor reference voltages. These voltages are used to fix the control of each PWM inverter.

Fig. 2 Illustration of the simplified diagram of the DFIG with VC.

3.2. Classical direct power control of DFIG

Direct power control (DPC) is established on the concept of direct torque control applied to AC machines. The principle of the DPC is to directly control the active and reactive power. The controllers used are hysteresis comparators for instantaneous active and reactive power

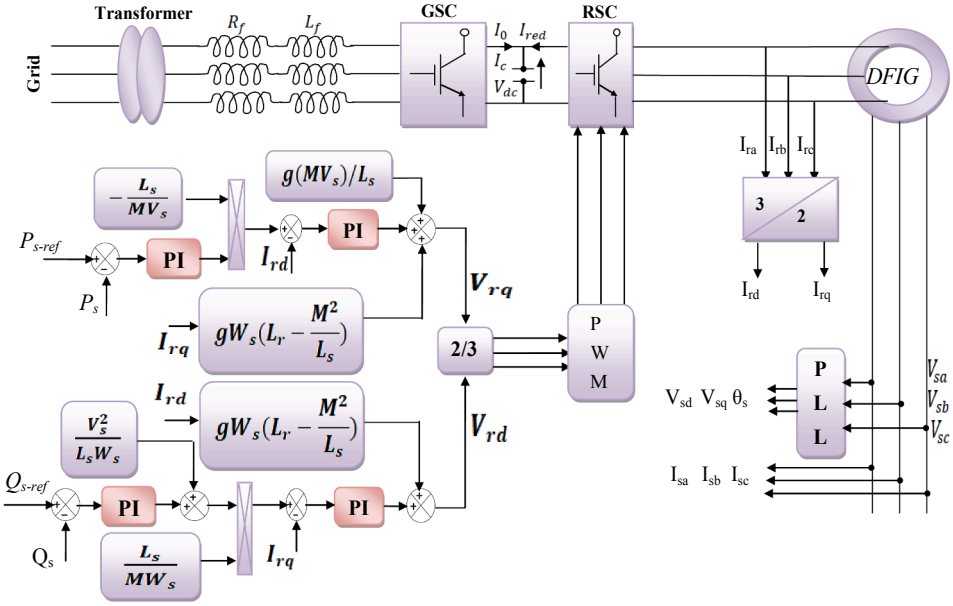

Fig. 2. Vector control of the DFIG.

errors. The output of the controllers with the sector where the position of the mains stator flux is located, constitute the inputs of a switching table.

The complex plane is divided into six angular sectors to determine the control sequence of the active and reactive powers with regard to the application of a stator voltage vector, Fig. 3.

A. Hysteresis power control

The stator flux module and the phase are given by [19]:

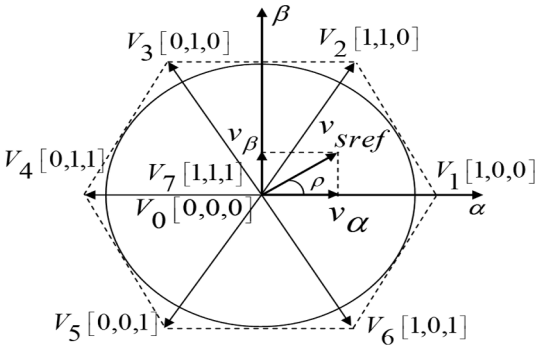

Fig. 3. Switching-voltage space vectors.

$$\begin{cases} |\Phi_s^r| = \sqrt{\Phi_\alpha^2 + \Phi_\beta^2} \\ \rho_r = \arctan\left(\frac{\Phi_{r\beta}}{\Phi_{r\alpha}}\right) \end{cases} \quad (11)$$

To generate the active and reactive powers switching states, the error between the estimated power and the reference one is the input of a three level hysteresis regulator. S_P (0,1) and S_Q (1,0, −1) as illustrated in Fig. 4. The errors in powers are estimated as:

$$\begin{cases} P_{s-error} = P_s^* - P_s \\ Q_{s-error} = Q_s^* - Q_s \end{cases} \quad (12)$$

B. Switching Table

Table 1 illustrate the change in the powers when the voltage vector is applied.

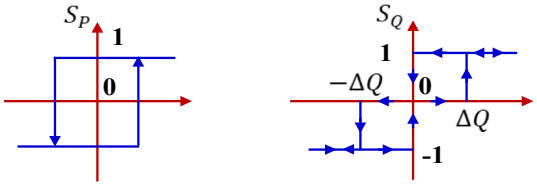

Fig.4. Hysteresis controller of active and reactive powers.

Selection of appropriate vector applied to the RSC is presented in the Table 2. This table established to control the active and reactive powers exchanged with grid.

The detailed structure of the classical DPC is depicted in Fig. 5.

The drawbacks of the classical DPC are the presence of the powers ripples. These ripples have an effect on the grid and the stress on the shaft of the turbine. It can lead to the destruction of the wind turbine. In the next section, we try to reduce these ripples by the proposition of an adaptive direct power control strategy.

Table 1
Generalized table of voltage vectors.

	Increase	Decrease
Reactive power	V_{k-1}, V_k, V_{k+1}	V_{k-2}, V_{k+2}, V_{k+3}
Active power	V_{k+1}, V_{k+2}	V_{k-2}, V_{k-1}

Table 2
Switching table for DPC of DFIG.

S_p		1			0		
S_q		−1	0	1	−1	0	1
ρ_r	1	V_6	V_0	V_2	V_5	V_7	V_3
	2	V_1	V_7	V_3	V_6	V_0	V_4
	3	V_2	V_0	V_4	V_1	V_7	V_5
	4	V_3	V_7	V_5	V_2	V_0	V_6
	5	V_4	V_0	V_6	V_3	V_7	V_1
	6	V_5	V_7	V_1	V_4	V_0	V_2

3.3. Adaptive direct power control

The principle of A-DPC is based on the analysis of the classical DPC switching table. It is known that increasing the torque (sector ρ_r) at a constant speed implies an increase in the power consumed by the machine. It is recalled here that the positive power is absorbed by the machine in motor mode while it is negative in generator mode. This relationship is also true in generator mode where an increase in torque reduces the power generated by the machine. Unfortunately, a great difficulty persists in the calculation of the angle of the rotor flux. In this respect, improved power control gives a robust means of knowing the current area of rotor flux.

The review of Table 2 illustrates that if the rotor flux was in sector 3 and the vector 4 had just been applied, the reactive power variation must necessarily be negative since the vector 4 increases reactive power supply to the rotor. If this is no longer possible, the sector estimate is wrong and the flux would be in sector 2 or 6. Given that it was previously in sector 3, so it would be unlikely to be in sector 6 now; since it would have skipped over to other sectors. The previous explanation can be represented using Tables 3 and 4 based on the Table 2.

In the case of inconsistency between expected and measured values. Table 4 suggest a modification of the current sector.

In the case where the flux is in the sector 3 and that, following the application of the vector 4, the variation of the stator reactive power has been positive, which is in contradiction with the Table 3, we suggest decrementing (-1) the current sector.

Fig. 6 represents the adaptation algorithm principle compared to the classical DPC.

The different steps of the A-DPC algorithm are established as follows:

- The first step: Initialization of the sector ρ_r before the update (for: ρ_r = 1: 6).

Table 3
Monitoring the change in reactive power.

Sector	V_0	V_1	V_2	V_3	V_4	V_5	V_6	V_7
1	0	−	−	+	+	+	−	0
2	0	−	−	−	+	+	+	0
3	0	+	−	−	−	+	+	0
4	0	+	+	−	−	−	+	0
5	0	+	+	+	−	−	−	0
6	0	−	+	+	+	−	−	0

- The second step: Initialization of the classical DPC vectors based on the Table 2 (for $V_i = V_0$: V_7).

Table 4
The update sectors.

Sector	V_0	V_1	V_2	V_3	V_4	V_5	V_6	V_7
1	0	0	−1	+1	0	−1	+1	0
2	0	+1	0	−1	+1	0	−1	0
3	0	−1	+1	0	−1	+1	0	0
4	0	0	−1	+1	0	−1	+1	0
5	0	+1	0	−1	+1	0	−1	0
6	0	−1	+1	0	−1	+1	0	0

- The third step: Monitoring the variability of the reactive power Qs Table 3. This table checks the state of reactive power variation. That is, it checks whether the variation of the reactive power measured at the stator corresponds to that expected for the sector and the current vector.
- The fourth step: Sector variation test, Table 4 based on the variation of the reactive power Table 3, if there is an inconsistency between the expected value and the measured value. Table 4 suggests a modification of the current sector.

Fig. 7 depicts the structure of the A-DPC of DFIG with variation in reactive power.

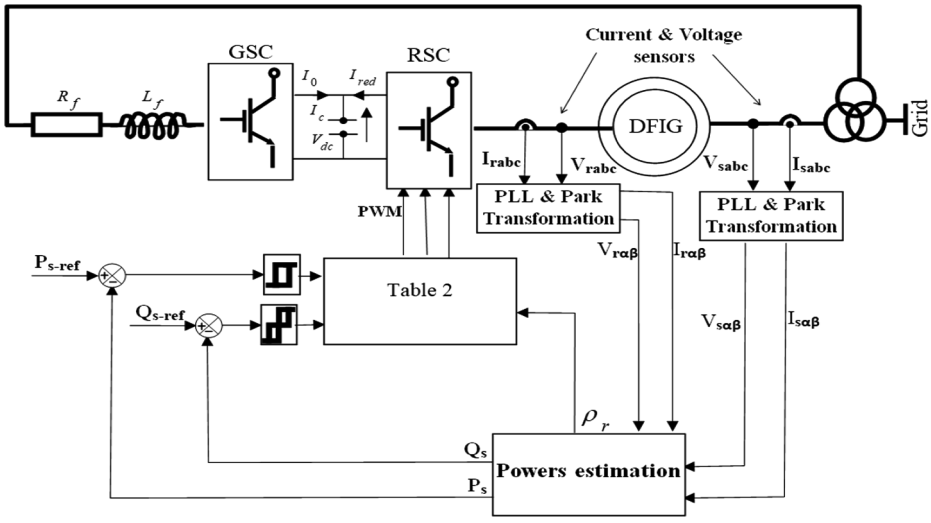

Fig. 5. Classical direct power control scheme of DFIG.

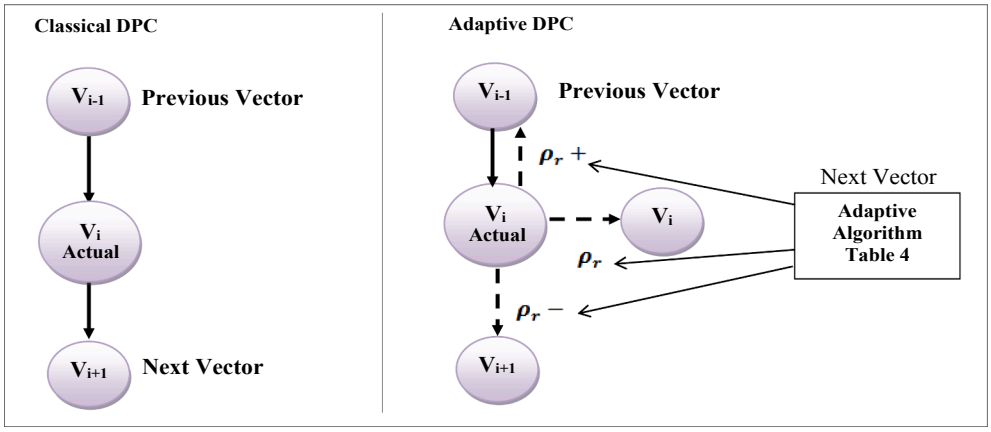

Fig. 6. Adaptive algorithm principle.

4. Results and discussion

Adaptive direct power control for double-Fed Induction generator has been introduced in this study. Different methods of DPC have been studied and realized using the Matlab/ Simulink software with the same operating conditions. The parameters of the DFIG and wind turbine are reported in Table 6. The wind speed profile used to test the three controllers is shown in Fig. 8. It consists of a set of 10 s data. The performance comparisons of the three algorithms are performed under the same operating conditions (sampling time, parametric variation).

4.1. Simulation results without parametric variation

The active powers produced by the DFIG controlled with VC, C-DPC, and A-DPC are presented in Fig. 9. In this figure, it can be noticed that the ripple is not the same for the three techniques. A zoom of the stator active powers for the three strategies is shown in Fig. 10. It is clear that the VC suffer from two problems: steady-state error and high active powers ripples. On the other hand, the A-DPC provides almost perfect behavior in tracking performance compared with the VC and C-DPC.

The stator reactive powers illustrated in Fig. 11 tracks the irreverence values very well; it can be seen that A-DPC shows improved performance than VC and C-DPC. This is clearly observed in Fig. 12. Using A-DPC the stator reactive powers' oscillations are lower, while with VC the dynamic is slower, due to the presence of the PI controllers and control loops.

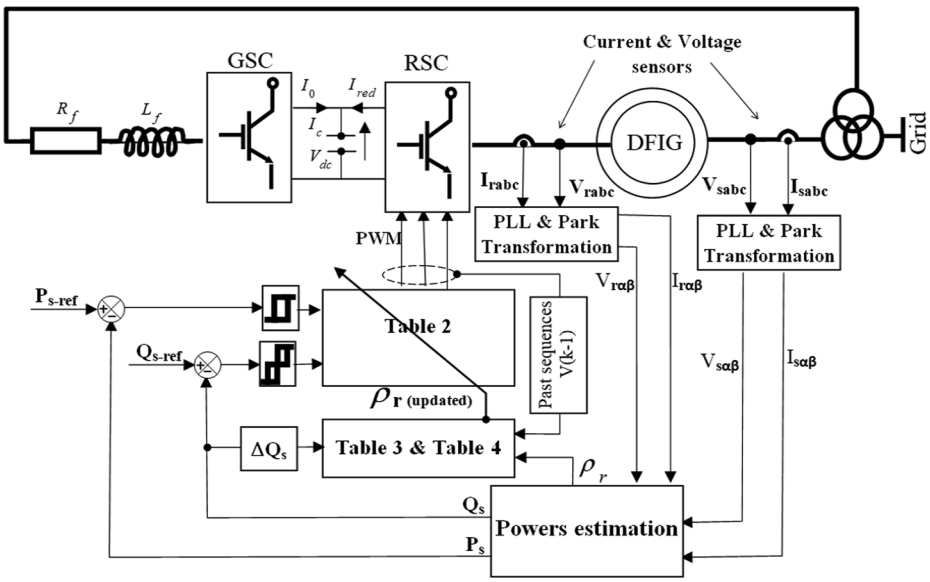

Fig. 7. Structure of the adaptive A-DPC of the DFIG with the variation of Qs.

In Fig. 13, the stator voltage and currents are sinusoidal and in opposite phases, the system is operating at rated conditions. The current is variable according to the variation of the active power, which varies according to the wind speed. It can be observed that the current ripple has also a notable reduction in A-DPC controller compared to the other controller.

Fig. 14 gives the stator current harmonic analysis. We can observe that the current harmonic distortion of the classical DPC is higher than A-DTC. It can be concluded that the suggested algorithm (A-DPC) gives a better performance with low THD.

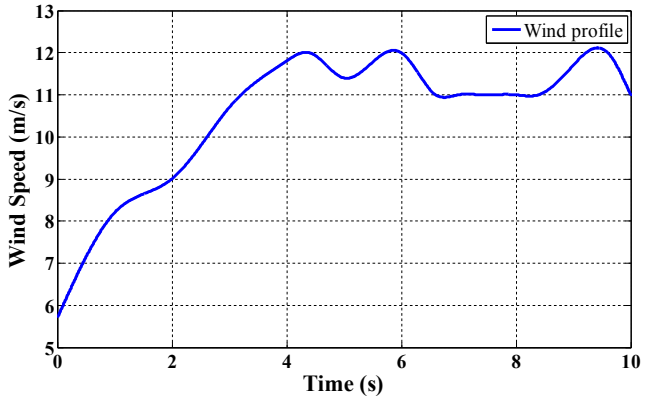

Fig. 8. Wind speed profile.

4.2. Simulation results with parametric variation + 150% on R_r and L_r

To study the effect of DFIG parameter uncertainty on the performances of the suggested (A-DPC), the rotor resistance R_r and inductance L_r parameter sensitivity are tested for the three schemes for + 150% variation at time t = 5 s, The powers are shown in Figs. 15, 16, 17 and 18. It can be observed from these figures that the (VC) and (C-DPC) schemes have a considerable error due to L_r and R_r variation. The proposed method is robust against parameter variations and allows a fast and suitable dynamic response.

Table 5 presents the quantitative analysis of the three approaches. The comparison among the presented techniques for power control implicates that the proposed (A-DPC) scheme gives much less chattering with a seamless transient response.

5. Conclusion

In this paper, a novel adaptive DPC for DFIG has been presented. The suggested control has been compared to the vector control and classical direct power control. Simulation results demonstrate that the powers' ripples and harmonic content of stator current are lower in (A-DPC) compared with other controls. The efficiency of the proposed DPC has been validated by simulation tests carried out with a 1.5 MW DFIG system. Moreover, to validate the influence of DFIG parameter variations on the performances of the proposed (A-DPC), the rotor resistance parameter sensitivity has been tested for the three schemes for + 150%

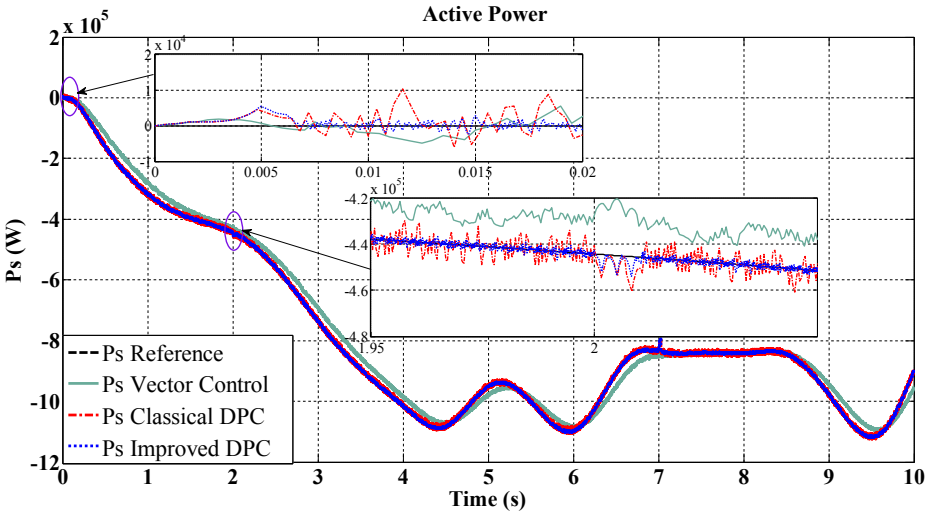

Fig. 9. Active power response under VC, C-DPC and A-DPC strategies.

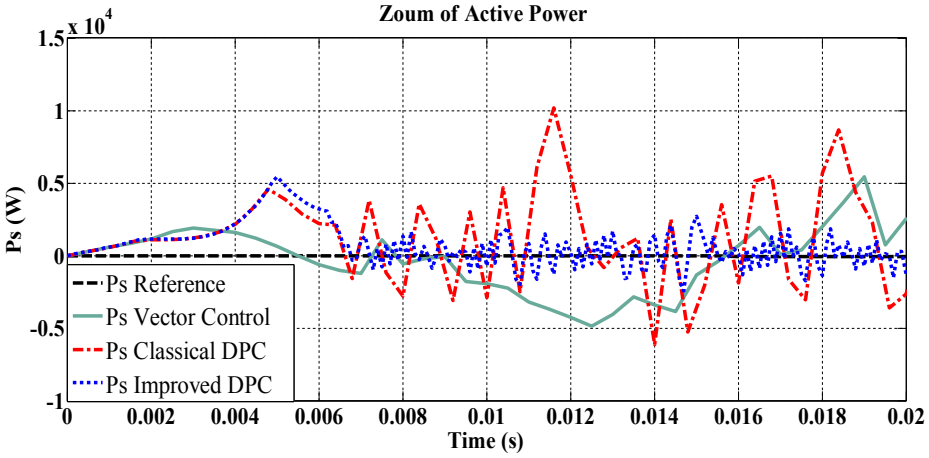

Fig. 10. Zoom of active power response under VC, C-DPC and A-DPC strategies.

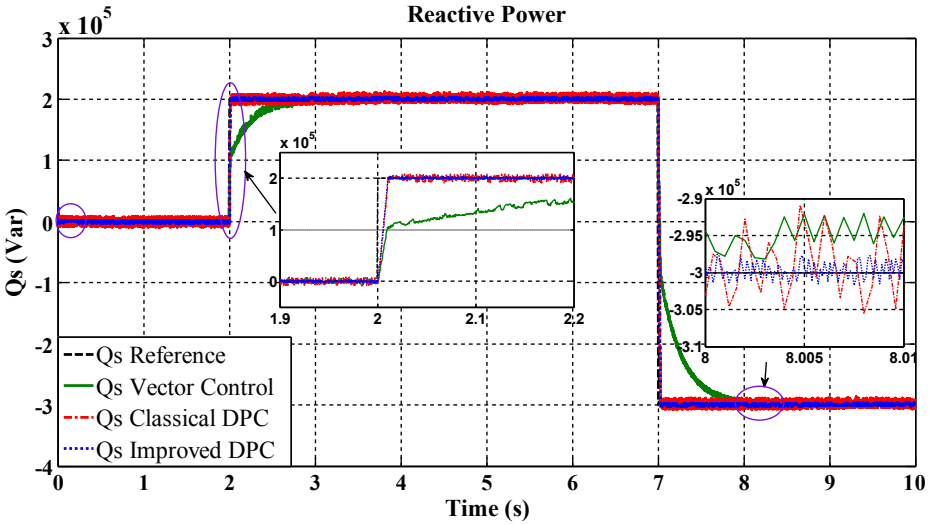

Fig. 11. Reactive power response under VC, C-DPC and A-DPC control strategies.

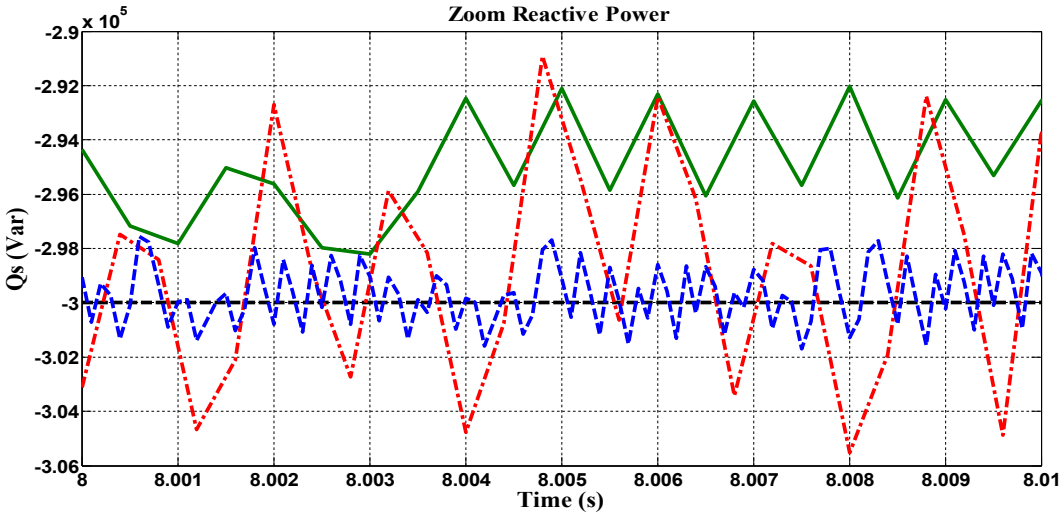

Fig. 12. Zoom of reactive power response under VC, C-DPC and A-DPC strategies.

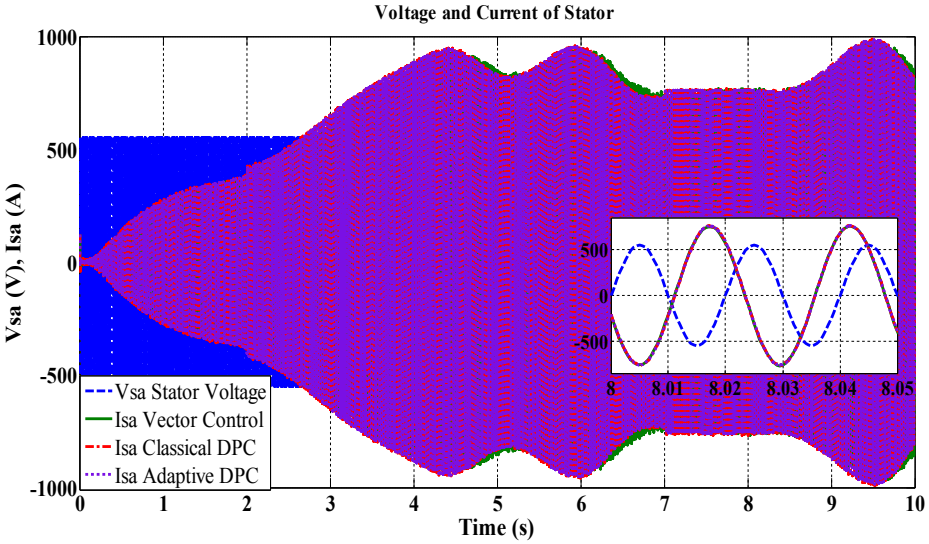

Fig. 13. Stator voltage V_{sa} and phase current I_{sa} of three approaches.

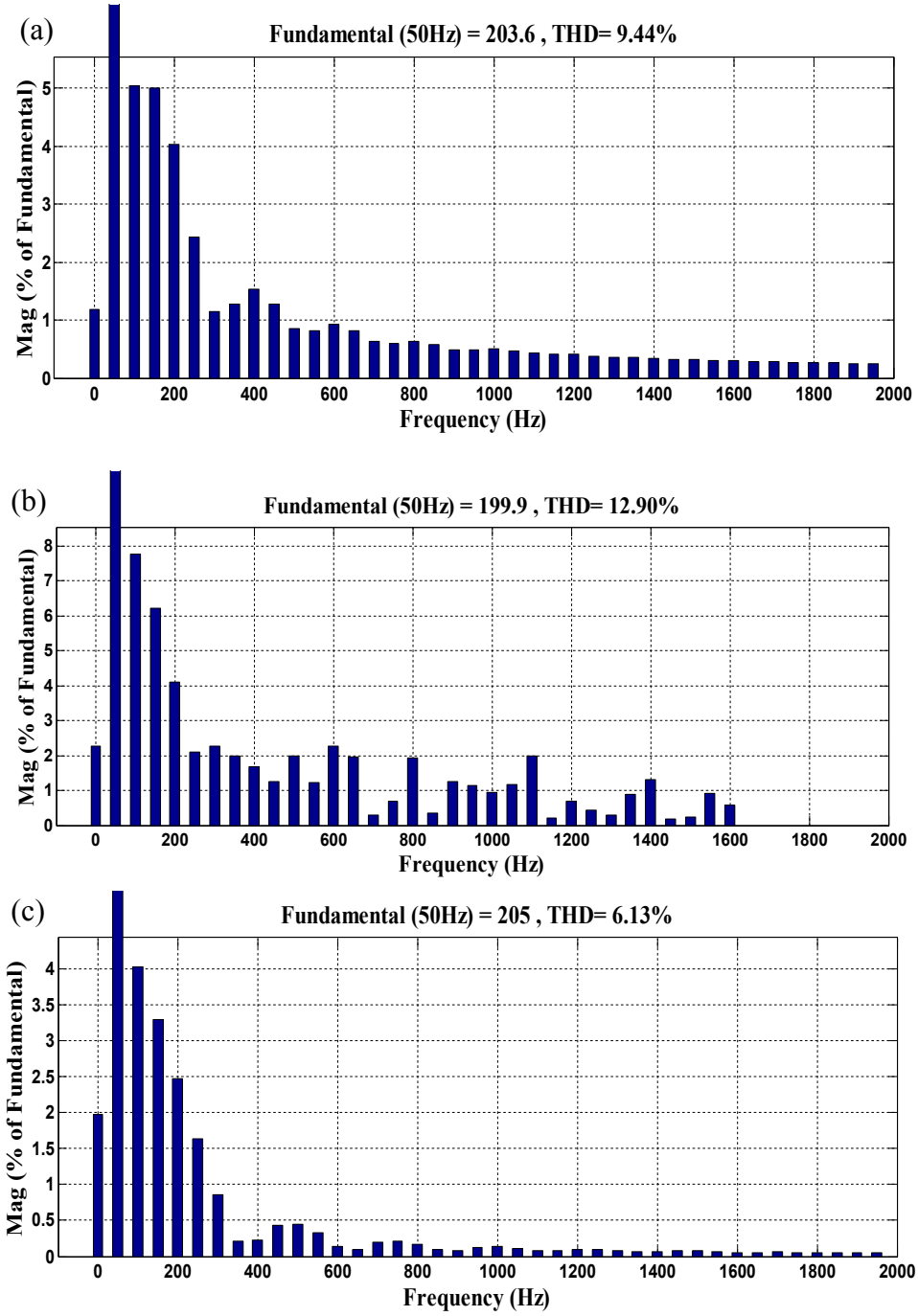

Fig. 14. Stator current FFT analysis, (a) conventional VC, (b) C-DPC, (c) A-DPC.

variations in rotor resistance and inductance; it has been shown that the (A-DPC) is robust and capable to reject the influences of uncertainty in system parameters. The proposed approach can be considered as an alternative solution to the control of DFIG.

The advantages of the proposed (A-DPC) are highlighted by the following points:

1. It does not require angular information of stator flux and synchronous coordinate transformations.
2. The transient responses and steady-state are insensitive to uncertainty parametric variation of the DFIG.
3. Enhanced transient performance.
4. Stator current harmonic spectra are improved.

Declaration of Competing Interest

Author declares that there is no conflicts of interest.

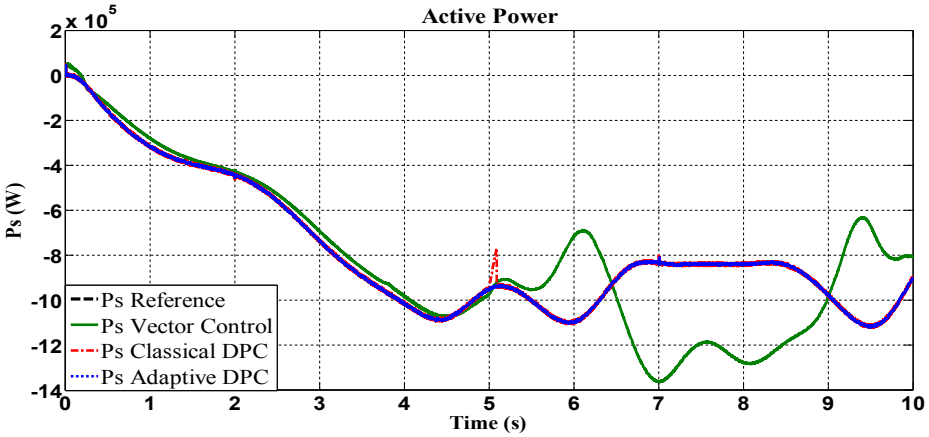

Fig. 15. Simulated results of stator active power.

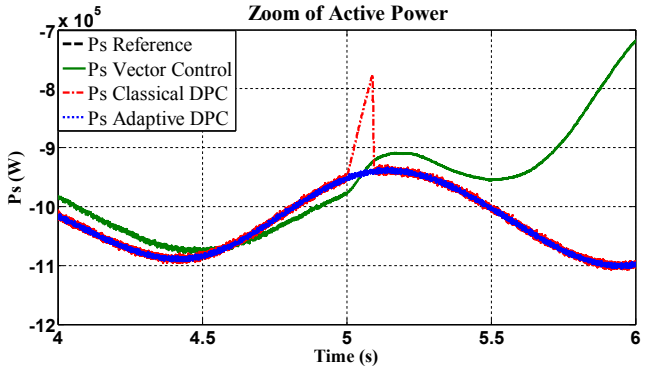

Fig. 16. Zoom of stator active power response under VC, C-DPC and A-DPC strategies.

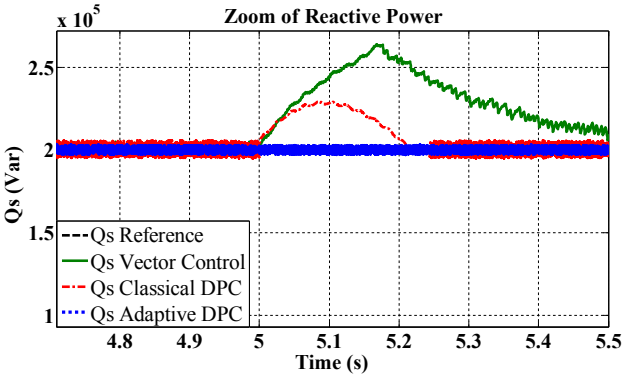

Fig. 18. Zoom of stator reactive power under VC, C-DPC and A-DPC.

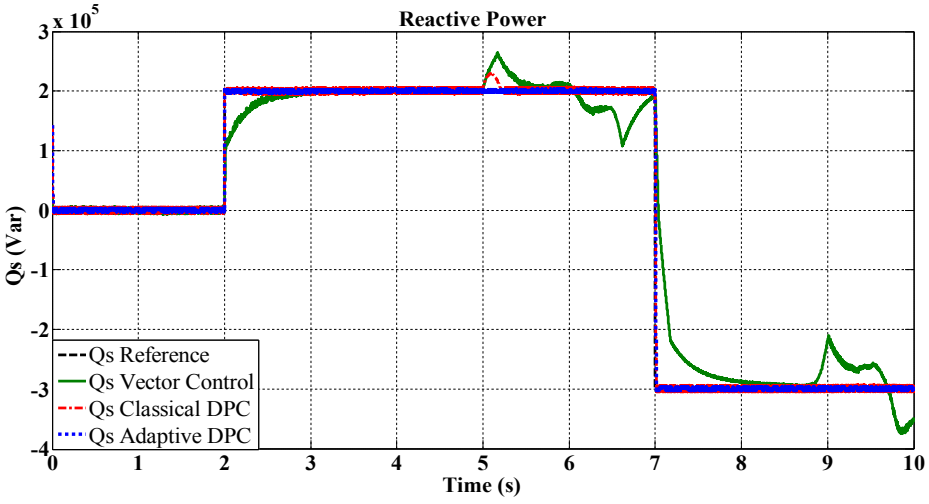

Fig. 17. Simulated results of stator reactive power.

Table 5
Performances comparison of the three controllers.

Approach	VC	C-DPC	A-DPC
Robustness to parameters mismatch	High	Medium	Low
Harmonic spectrum of stator current	Medium	High	Low
Chattering	Medium chattering	Considerable chattering	Small chattering
Transient performance of the active power	Relatively fast with medium settling time	Relatively fast with low settling time	Fast with low settling time
Rising time of the active power	0.009 s	0.007 s	0.004 s
Transient performance of the reactive power	Relatively fast with medium settling time	Relatively fast with low settling time	Fast with low settling time
Rising time of the reactive power	0.011 s	0.007 s	0.005 s
ImplementationComplexity	High	Low	Low

Table 6
Wind turbine and DFIG parameters.

DFIG Parameters		Wind Parameters	
Rated power, P_n	1.5 MW	Blade radius, R	35.25 m
Stator voltage, V_s	398/690 V	Number of blades	3
Rates current, I_n	1900 A	Gearbox ratio, G	90 m
DC-link voltage U_{DC}	1200 V	Inertia moment, J	1000 Kg m^2
Stator frequency, f	50 Hz	friction coefficient, *f*	0.0024 N m s^{-1}
Stator inductance, L_s	0.0137 H	Cut-in wind speed	4 m/s
Rotor inductance, L_r	0.0136 H	Cut-out wind speed	25 m/s
Mutual inductance, M	0.0135 H	Nominal wind speed, *v*	16 m/s
Stator resistance, R_s	0.012 Ω		
Rotor resistance, R_r	0.021 Ω		
Number of pole pairs P	2		

References

[1] Ackermann T. Wind Power in Power Systems. John Wiley and Sons; 2005.
[2] Wanger H, Mathur J. Introduction to wind energy systems. Green Energy and Technology. Berlin Heidelberg: Springer; 2013.
[3] Edrah M, Lo KL, Anaya-Lara O. Impacts of high penetration of DFIG wind turbines on rotor angle stability of power systems. IEEE T Sustain Energy 2015;6(3):759–66.
[4] Tazil M, Kumar V, Kong S. Three-phase doubly fed induction generator: an overview. IET Electr Power Appl 2009;4(2):75–89.
[5] El Makrini Y, El Karkri Y. LVRT control strategy of DFIG based wind turbines combining passive and active protection. Int J Renew Energy Res 2017;7(3):1259–69.
[6] Cárdenas R, Peña R, Alepuz S, Asher G. Overview of control systems for the operation of DFIGs in wind energy applications. IEEE Trans Ind Electron 2013;60(7):2776–98.
[7] Bianchi FD, Batista HD, Mantz RJ. Wind turbine control systems: principles, modelling and gain scheduling design: advances in industrial control. Springer; 2006.
[8] Haiqiang Z, Ping JU, Yusheng X, Jie Z. Probabilistic equivalent model of DFIG-based wind farms and its application in stability analysis. J Mod Power Syst Clean Energy 2016;4(2):248–55.
[9] Shifeng W, Sicong W. Impacts of wind energy on environment: a review. Renew Sustain Energy Rev 2015;49:437–43.
[10] Aydin E, Polat A, Ergene LT. Vector control of DFIG in wind power application. 5th international conference on renewable energy research and applications (ICRERA' 2016), Birmingham, UK. 2016.
[11] Reddak M, Berdai A, Gourma A, Boukherouaa J. An improved control strategy using RSC of the wind turbine based on DFIG for grid harmonic currents mitigation. Int J Renew Energy Res 2018;8(1):266–73.
[12] Amrane F, Chaiba A, Babes BE, Mekhilef S. Design and implementation of high performance field oriented control for grid connected doubly fed induction generator via hysteresis rotor current controller. Rev Roum Sci Techn – Électrotechn Et Énerg 2016;61(4):319–24.
[13] Mohammadi J, Vaez-Zadeh S, Afsharnia S, Daryabeigi E. A combined vector and direct power control for DFIG-based wind turbines. IEEE Trans Sustain Energy 2014;5(3):767–75.
[14] Li S, Haskew TA, Williams KA. Watloski R.P.S. Control of DFIG wind turbine with direct-current vector control configuration. IEEE Trans Sustain Energy 2012;3:1.
[15] Tamalouzt S, Kassa I, Toufik R, Abdessemed R. Direct torque control of wind turbine driven doubly fed induction generator. Rev Roum Sci Techn Électrotechn Et Énerg 2016;61(3):244–9.
[16] Mazouz F, Belkacem S, Harbouche Y, Abdessemed R, Ouchen S. Active and reactive power control of a DFIG for variable speed wind energy conversion. IEEE 6th International conference on systems and control (ICSC'2017), Algeria. 2017.
[17] Nadour M, Essadki A, Nasser T. Comparative analysis between PI & backstepping control strategies of DFIG driven by wind turbine. Int J Renew Energy Res 2017;7(3):1308–16.
[18] Weng YT, Hsu YY. Reactive power control strategy for a wind farm with DFIG. Renew Energy 2016;94(C):383–90.
[19] Mazouz F, Bezzou A, Belkacem S. DPC of the doubly fed induction generator based on the WECS. 3rd International Conference on Power Electronics and their Applications (ICPEA 2017), Djelfa, Algeria. 2017.
[20] Varzaneh SG, Abedi M, Gharehpetian G. A new simplified model for assessment of DFIG-based wind farm participating in frequency control system. Electric Power Syst Res 2017;148:220–9.
[21] Arjang YT, Edris P, Bo NJ. Active and reactive power ripple minimization in direct power control of matrix converter-fed DFIG. Electr Power Energy Syst 2014;63:600–8.
[22] Gadouche Z, Cheikh B, Allaoui T, Belabbas B. Speed-sensorless DFIG wind turbine for power optimization using fuzzy sliding mode observer. Int J Renew Energy Res 2017;7(2):614–21.
[23] Belfedal C, Moreau S, Champenois G, Allaoui T, Denai M. Comparison of PI and direct power control with SVM of doubly fed induction generator. J Electr Electron Eng 2008;8(2):633–41.
[24] Sarat KS, Balamurugan M, Krishna PL, Prabhakar SK. Comparison of SVM and DPC for reactive power control of DFIG based wind energy systems. Int J Renew Energy 2016;11(1):1614–21.
[25] Mariusz M, Marek J, Kazmierkowski MP. Simple direct power control of three-phase PWM rectifier using space-vector modulation (DPC-SVM). IEEE Trans Ind Electron 2004;51(2):447–54.
[26] Myna, B. Direct Power Control of Three-Phase PWM Rectifier using Space- Vector Modulation (DPC- SVM), Thesis, 2017.
[27] Gui Y, Kim C, Chung CC, Guerrero JM, Guan Y, Quintero JCV. Improved direct power control for grid-connected voltage source converters. IEEE Trans Ind Electron 2018;65(10):8041–51.
[28] Tremblay E. Contribution à la commande de l'éolienne à MADA en permettant l'amélioration de la qualité d'onde du réseau électrique. Maitrise en génie électrique, 2009.
[29] Bennouk A, Nejmi A, Ramzi M. Stability enhancement of a wind plant based on a DFIG and a PMSM: a lyapunov approach. Energy Rep 2018;4:13–22.
[30] Aitouche A, Ghorbani R, Bayart M. Robust nonlinear control of wind energy conversion systems. Int J Elect Power Energy Syst 2013;44(1):202–9.
[31] Xiong P, Sun D. Backstepping-based DPC strategy of a wind turbine-driven DFIG under normal and harmonic grid voltage. IEEE Trans Power Electron 2016;31(6):4216–25.
[32] Mazouz F, Belkacem S, Harbouche Y, Abdessemed R, Ouchen S. Fuzzy control of a wind system based on the DFIG. International Conference on Artificial Intelligence in Renewable Energetic Systems IC-AIRES 2017, Tipaza Algeria. 2017.
[33] Djilali L, Sanchez EN, Belkheiri M. Neural input-output feedback linearization control of a DFIG based wind turbine. IFAC 2017;50(1):11082–7.
[34] Yang B, Yu T, Shu H, Dong J, Jiang L. Robust sliding-mode control of wind energy conversion systems for optimal power extraction via nonlinear perturbation observers. Appl Energy 2018;210(C):711–23.
[35] Mazouz F, Belkacem S, Colak I, Drid S. Direct power control of DFIG by sliding mode control and space vector modulation. 7th International conference on system and control, IEEE (ICSC), Valencia – Spain. 2018.
[36] Lhachimi H, Sayouti Y, El Kouari Y. Optimal improvement of direct power control strategy based on sliding mode controllers. Comput Electr Eng 2018;71:637–56.
[37] Elnady A, Al-ShabiM. Operation of direct power control scheme in grid-connected mode using improved sliding mode observer and controller. Int J Emerg Electr Power Syst 2018:1–18.
[38] Matraji I, Al-Durra A, Errouissi R. Design and experimental validation of enhanced adaptive second-order SMC for PMSG-based wind energy conversion system. Electr Power Energy Syst 2018;103:21–30.
[39] Phan DC, Yamamoto S. Rotor speed control of doubly fed induction generator wind turbines using adaptive maximum power point tracking. Energy 2016;111:377–88.
[40] Liu J, Meng H, Hu Y, et al. A novel MPPT method for enhancing energy conversion efficiency taking power smoothing into account. Energy Convers Manage 2015;101:738–48.
[41] Chatrenour N, Razmi H, Doagou MH. Improved double integral sliding mode MPPT controller based parameter estimation for a stand-alone photovoltaic system. Energy Convers Manage 2017;139:97–109.
[42] Bektache A, Boukhezzar B. Nonlinear predictive control of a DFIG-based wind turbine for power capture optimization. Electr Power Energy Syst 2018;101:92–102.
[43] Darabian M, Jalilvand A. Predictive control strategy to improve stability of DFIG-based wind generation connected to a large-scale power system. Int Trans Electr Energy Syst 2017;25(5):2110–25.
[44] Errouissi R, Al-Durra A, Muyeen SM, Leng S, Blaabjerg F. Offset-free direct power control of DFIG under continuous-time model predictive control. IEEE Trans Power Electron 2017;32(3):2265–77.
[45] Chhor J, Tourou P, Sourkounis C. On Advanced control strategies for DFIG-based wind energy conversion systems during voltage unbalance. 6th international conference on renewable energy research and applications ((ICRERA' 2017), San Diego, CA, USA. 2017. p. 5–8.
[46] Zandzadeh J, Vahedi AM. Improvement of direct power control of DFIG under unbalanced grid voltage condition. Electr Power Energy Syst 2014;59:58–65.
[47] Farshadnia M, Seyed Abbas T. Current-based direct power control of a DFIG under unbalanced grid voltage. Electr Power Energy Syst 2014;62:571–82.